ANALYSIS OF TRANSIENT EMBANKMENT STABILITY USING THE DYNAMIC PROGRAMMING METHOD

Gilson Gitirana Jr, University of Saskatchewan, Saskatoon, Canada
Delwyn G. Fredlund, University of Saskatchewan, Saskatoon, Canada

ABSTRACT: Conventional limit equilibrium methods of slope stability analysis are usually combined with restrictions to the slip surface shape. The Dynamic Programming Method (DPM) of slope stability analysis represents an important breakthrough in that these restrictions are significantly relaxed. This paper presents the analysis of transient embankment stability using a computer model based on the DPM, combined with finite element stress and pore-water pressure fields. The problem studied contains sharp wetting fronts and a significant, nonlinear spatial variation of shear strength. The analyses results indicate that the DPM model is robust, fast, and stable. The stability analysis using the DPM shows that the slip surface shape is affected by infiltration and deviates from a circular shape in some cases. Poisson ratio was found to have an influence on the shape of critical slip surfaces and the factors of safety.

RESUME: Les méthodes conventionnelles d'équilibre limite d'analyse de stabilité de talus sont combinées avec restrictions à la forme de surface de glissade. La méthode de programmation dynamique (DPM) d'analyse de stabilité de talus représente une percée importante parce que ces restrictions sont sensiblement détendues. Cet article présente l'analyse de la stabilité d'un remblai en utilisant un modèle d'ordinateur basé sur le DPM, combinée avec champs de contraintes et pressions interstitielles d'élément finis. Le problème étudié contient fronts de mouillage accentuée et grande variation spatiale de la résistance au cisaillement. Les résultats des analyses indiquent que le DPM modèle est robuste, rapide, et stable. L'analyse de stabilité employant le DPM montre que la forme de la surface de glissade est affectée par l'infiltration et dévie d'une forme circulaire dans certains cas. Le rapport de Poisson a une influence importante sur la forme des surfaces critiques de glissade et de leurs coefficients de sécurité.

1. INTRODUCTION

This paper presents the application of the *Dynamic Programming Method* to the analysis of stability of embankments subjected to transient moisture flow. The study is based on a hypothetical embankment comprised of lacustrine silt and subjected to a continuous rainfall during four uninterrupted days. A Dynamic Programming algorithm called SAFE-DP (Stability Analysis using Finite Element stress fields and Dynamic Programming) has been developed. The stresses and pore-water pressures utilized in the stability analyses are calculated solving the partial differential equations (PDE's) for equilibrium and moisture flow. A general purposed solver called FlexPDE (PDE Solutions Inc. 2003) was used to solve the PDE's. The stability, robustness, and accuracy of the software code was investigated using a hypothetical case and three different values of Poisson ratio. The evolution of the shape and position of the slip surface and the resultant factors of safety are presented and analysed.

2. STABILITY ANALYSIS USING DYNAMIC PROGRAMMING

2.1 Previous Studies Related to Slope Stability Analysis Using Dynamic Programming

The *Dynamic Programming Method* (DPM) has been the subject of interest of a number of researchers, since the 80's. Baker (1980) applied the DPM to the analysis of slope stability, while retaining the Spencer (1967) assumption regarding interslice forces. Yamagami and Ueta (1988) extended the DPM approach and replaced the Spencer limit equilibrium method with stresses computed in a finite element (FE) stress analysis. More recent DPM studies have been presented by Zou et al. (1995) and Pham et al. (2002).

The DPM is a general method of maximization and minimization of linear (additive) functionals (Bellman 1957). Conventional limit equilibrium methods are usually combined with an assumption regarding the shape of the critical slip surface. The DPM represents an important breakthrough in that the slip surface shape restrictions are significantly relaxed. The combined use of finite element stress fields further enhances the analysis by providing means of incorporating into the slope stability analysis more realistic boundary conditions, soil stress-strain properties, and stress history. Little human interference in the analysis process is required once the problem geometry, boundary conditions, material properties, and search grid are established.

The input requirements of the DPM combined with FE stress fields are quite similar to those of conventional limit equilibrium methods. The stress-strain constitutive parameters and the boundary conditions are the only additional parameters that must be designated. Studies to-date have shown that the elastic parameters need only to be approximate, in general, and that the Poisson's ratio has a modest influence on the results (Pham 2002). The use of problem solving environments, such as FlexPDE, can make stress-strain analyses as easy as traditional limit equilibrium procedures. If a linear constitutive law is adopted in the stress analysis, the computational time can be similar to, or shorter than that of conventional limit equilibrium codes (Pham et al. 2001).

2.2 Optimization Procedure

Figure 1 presents the analytical scheme for stability analysis using the Dynamic Programming Method, DPM (Yamagami and Ueta 1988 and Pham et al. 2001). The procedure is based on the assumption that the critical slip surface can be approximated by "*n*" linear segments. Each linear segment connects two *state points* located at two successive *stages*. The *search grid* consists of a collection of *state points* lying on "*n*+1" *stages*. A relatively coarse search grid is superimposed on the geometry shown in Figure 1. The dynamic programming procedure is used to determine a continuous assemblage of segments that corresponds to a minimum overall factor of safety. In order to quantify the overall stability, a *factor of safety*, F_s, along a slip surface is defined in its discrete form as:

$$F_s = \sum_{i=1}^{n} R_i \Big/ \sum_{i=1}^{n} S_i = \sum_{i=1}^{n} \tau_{f_i} \Delta L_i \Big/ \sum_{i=1}^{n} \tau_i \Delta L_i \qquad [1]$$

where n is the total number of segments; R_i is the resisting force of the soil along the i^{th} segment, kN/m; S_i is the shear force acting along the i^{th} segment, kN/m; τ_{fi} is the shear strength of the soil along the i^{th} segment, kPa; ΔL_i is the length of the i^{th} segment, m; and τ_i is the shear stress along the i^{th} segment, kPa. This definition of factor of safety (i.e., considering the state of overall limit equilibrium of forces), puts the DPM within a similar class to the limit equilibrium methods.

The unique characteristic of the DPM lies in the manner by which the shape and position of the critical slip surface, along with the corresponding minimum F_s, is obtained. The dynamic programming method can only be applied to *additive functionals* (i.e., functions of the form $Y = \Sigma[a \cdot y_i + b]$). For that reason, in order to minimize the non-additive F_s functional the following additive functional is introduced (Baker, 1980):

$$G = \sum_{i=1}^{n} (\tau_{f_i} \Delta L_i - F_s \tau_i \Delta L) \qquad [2]$$

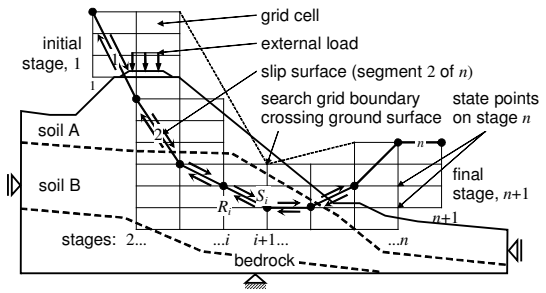

Figure 1. The analytical scheme for stability analysis using Dynamic Programming.

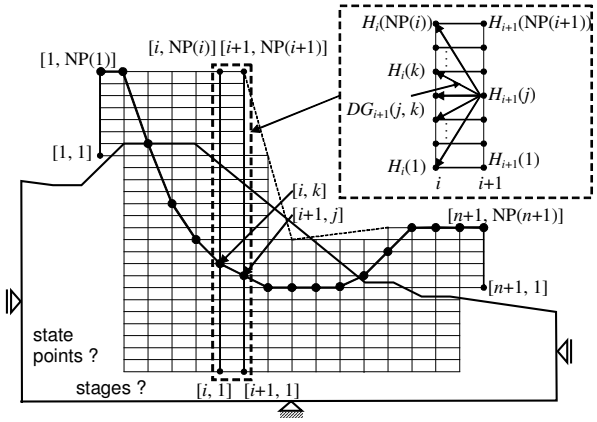

Figure 2. Optimum functions: detail showing two adjacent stages.

In order to minimise G, the *optimal function*, H, is used. $H_{i+1}(j)$ is defined as the minimum of G between any *state point* at the initial *stage* and any posterior *state point* [i, j]. According to the principle of optimality (Bellman 1957), the optimal function at a posterior stage, $H_{i+1}(j)$, is a function of the optimal function at the prior stage, $H_i(k)$, as follows:

$$H_{i+1}(j) = \min\left[H_i(k) + DG_{i+1}(j,k)\right] \qquad [3]$$

where i = 1, n; j = 1, NP(i+1); k = 1, NP(i); NP(i) is the number of *state points* on *stage* i; and $DG_{i+1}(j,k) = \tau_{f_j} \Delta L_i - F_s \tau_i \Delta L$. The optimization scheme described by Eq. 3 is presented in Fig 2. The term $DG_{i+1}(j, k)$ corresponds to the 'cost' of passing between the state points [i+1, j] and [i, k], and is termed the *return function*. The principle of optimality establishes that the optimal function at each state point of a posterior stage corresponds to the minimum value amongst all the sums of the optimal functions at each state point of the prior stage and the 'costs' of passing between the state points [i+1, j] and [i, k]. A more rigorous examination of the principle of optimality can be found in Bellman (1957).

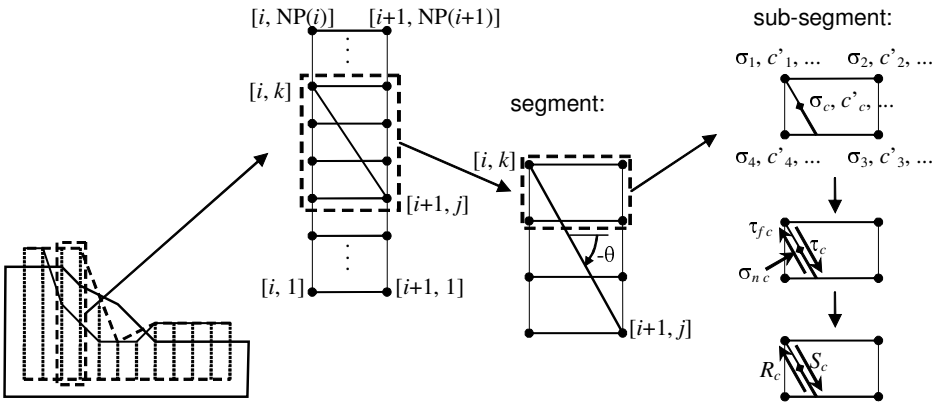

Figure 3. Optimum variables on a segment connecting two state points.

The principle of optimality implies in a sequential computation that starts on the first stage and goes towards the last stage. At the initial stage, the value of the optimal function, $H_1(k)$, must be set equal to zero. The search for the optimal function $H_{i+1}(j)$ must be repeated for each state point in each stage, up to the last stage, n+1.

The ultimate minimum value of G corresponds to the minimum value of H at n+1, min[$H_{n+1}(j)$]. The optimal path that defines the critical slip surface is found by connecting the optimal state points, traced back from the final stage to the initial stage. The value of F_s is given an assumed value for the first slip surface computation and replaced by the newly obtained F_s. This process must be repeated until F_s converges to a unique value while respecting an error tolerance.

The search grids presented in Figs. 1 and 2 observe certain rules. The state points at the initial and final states (1 and n+1) must all be above the ground surface in order for the slip surfaces to form a complete wedge of soil. There must be state points at the intermediate stages both above and below the ground surface, giving freedom for the slip surface to find its most critical position without improper grid restrictions. Finally, the search grid must cross the ground surface somewhere along the intermediate stages in order to force slip surfaces to cross the ground surface.

2.3 Shear Strength and Stresses within the DPM Search Grid

The shear strength, normal stress, and acting shear stress at any *state point* must be determined in order to solve Eqs. 2 and 3. These variables can be calculated based on the finite element stress field, pore-water pressure field, shear strength parameters, and orientation angle of the plane. The stress field is obtained by solving the PDE's governing static equilibrium. The pore-water pressure field is determined by solving the PDE's governing water movement along with appropriate soil-atmospheric boundary conditions. If a regular search grid formed by rectangular grid cells is used (see Figs. 1 and 2), it is convenient to interpolate the values of the variables involved on a regular *data grid* coinciding with the search grid. The variables interpolated are the stress state, pore-water pressure, and shear strength parameters. The data grid must extend beyond the area of the soil domain, overlapping the entire area enclosed by both the search grid and the soil domain. A value of zero must be assigned to the values of the variables on grid points not inside the soil mass.

Figure 3 presents how the variables on any segment connecting two state points can be calculated from the data grid. The values of any variable along any segment can be considered approximately equal to the value interpolated at the centre of the segment. If a segment crosses more than one grid cell, the value of the variables must be interpolated at the centre of each 'sub-segment' within each cell. The interpolation can be performed using Lagrange interpolation functions for linear rectangular elements. The subscript 'c' in Fig. 3 indicates that the variable lies on the sub-segment centre. Once the values of the variables at the centre of the sub-segments are determined, the values of τ_{fi}, σ_{ni}, and τ_i may be calculated. The resisting forces, R_i, and actuating shear forces, S_i, at each segment are equal to the sum of R_c and S_c at each sub-segment, respectively. R_c and S_c are determined by multiplying the shear stress and shear strength by the corresponding sub-segment lengths.

The shear strength, τ_{fi}, can be determined by using the shear strength envelope for a saturated/unsaturated soil (Fredlund and Rahardjo 1993). The shear strength with respect to soil suction can be based on a prediction technique dependent upon the SWCC. The normal stress, σ_{ni}, and shear stress, τ_i, acting on a plane inclined at an angle θ can be computed from the stress state defined by σ_x, σ_y, and τ_{xy}:

$$\sigma_{n_i} = \sigma_x \sin^2\theta + \sigma_y \cos^2\theta - \tau_{xy} \sin 2\theta \qquad [4]$$

$$\tau_i = [(\sigma_x - \sigma_y)/2] \sin 2\theta - \tau_{xy} \cos 2\theta \qquad [5]$$

where σ_x and σ_y are the total normal stresses acting on the *x*- and *y*-directions, respectively; and τ_{xy} is the total shear stress acting on the *x*-plane and *y*-direction. The normal stress, σ_{ni}, (Eq. 4) is later used in the calculation of shear strength. The actuating shear stress, τ_i, (Eq. 5) is required in the factor of safety equation.

3. PARTIAL DIFFERENTIAL EQUATIONS GOVERNING SOIL BEHAVIOUR

The moisture flow and static equilibrium of the soil comprising an embankment can be represented by a system of partial differential equations (PDE's). The PDE's are obtained from basic continuity and equilibrium laws, combined with constitutive laws that describe soil behaviour.

3.1 Conservation and Flow of Water

The conservation of mass equation for the water phase can be derived by taking the rate of flux of water mass in and out of a representative elemental volume (REV) and equating the difference to the rate of change of water mass within the element with time. For two-dimensional flow only flow in the *x*- and *y*-directions are considered. The mass flux of liquid water in saturated/unsaturated soils can be described by using Darcy's law. The volume of water within the REV can be expressed in terms of the stress state variables. The coefficient of water volume change can be written as the derivative of the soil-water characteristic curve. Combining the conservation of mass equation, the constitutive water and air flow law, and the derivative of the soil-water characteristic curve, the following PDE is obtained:

$$\frac{\partial}{\partial x}\left[k^w \frac{\partial\left(u_w/\gamma_w\right)}{\partial x}\right]+\frac{\partial}{\partial y}\left[k^w \frac{\partial\left(u_w/\gamma_w+y\right)}{\partial y}\right]=-m_2^w \frac{\partial u_w}{\partial t} \quad [6]$$

where k^w is the hydraulic conductivity ($k^w = f(u_a\text{-}u_w)$, m/s); u_a is the pore-air pressure, kPa; u_w is the pore-water pressure, kPa; γ_w is the unit weight of water, ≈ 9.81 kN/m3; y is the elevation, m; m_2^w is the coefficient of water volume change with respect to matric suction, $m_2^w = \left(e/(1+e)\right)\left(dS/d(u_a-u_w)\right)$, 1/kPa; and e is the void ratio. Two unsaturated soil property functions can be identified in Eq. 6; namely: the hydraulic conductivity and the coefficient of water volume change. These soil properties functions vary with soil suction, and therefore, the PDE is physically non-linear.

3.2 Static Equilibrium of Forces and Stress-Strain Relationship

The PDE's governing static equilibrium of forces can be obtained by considering the equilibrium of forces acting upon a REV of soil. For the two-dimensional case, equilibrium in the *x*- and *y*-directions must be considered. The forces are expressed in terms of stresses and infinitesimal areas. Combining the equilibrium equations with Hooke's generalised stress-strain law, and expressing the strain in terms of small displacements, the following PDE's are obtained for the *x*- and *y*-directions:

$$\frac{\partial}{\partial x}\left[D_{11}\frac{\partial u}{\partial x}+D_{12}\frac{\partial v}{\partial y}\right]+\frac{\partial}{\partial y}\left[D_{44}\left(\frac{\partial u}{\partial y}+\frac{\partial v}{\partial x}\right)\right]=0 \quad [7]$$

$$\frac{\partial}{\partial x}\left[D_{44}\left(\frac{\partial u}{\partial y}+\frac{\partial v}{\partial x}\right)\right]+\frac{\partial}{\partial y}\left[D_{12}\frac{\partial u}{\partial x}+D_{11}\frac{\partial v}{\partial y}\right]+\gamma=0 \quad [8]$$

where u and v are the displacement in the *x*- and *y*-directions respectively, m; $D_{11}=E(1\text{-}\mu)/[(1+\mu)(1\text{-}2\mu)]$; $D_{12}=E\mu/[(1+\mu)(1\text{-}2\mu)]$; ; $D_{44}=E/[2(1+\mu)]$; E is the Young modulus, kPa; μ is the Poisson ratio; $\gamma=\left(G_s+Se\right)\gamma_w/(1+e)$ is the unit weight of the soil, kN/m^3; and G_s is the specific unit weight of soil particles. Volume change due to changes in pore-water pressure is neglected in Eqs. 7 and 8.

In order to solve these PDE's governing flow of moisture and static equilibrium a multi-purpose partial differential equation solver is used, FlexPDE (PDE solutions 2003). FlexPDE uses the finite element (FE) and the finite difference (FD) methods combined with Newton-type methods of solution of non-linear coupled systems. FlexPDE has friendly input and output features combined with automatic mesh generation, time-step control, and choice of non-linear approaches.

4. EMBANKMENT STABILITY ANALYSIS

The stability of a hypothetical embankment comprised of lacustrine silt and subjected to heavy rainfall conditions was analysed for a period of 4 days. In order to determine the embankment stability along the time, the pore-water pressure distribution was sampled at several pre-determined instants, t = 0, 12, 24, 36, 48, 60, 72, 84, and 96 hours. The degree of saturation within the soil mass and the soil unit weight distribution were computed as functions of the pore-water pressure distribution (i.e., the SWCC). For each of the chosen sampling times, the partial differential equations governing static equilibrium were solved using the soil unit weight distribution. Finally, the Dynamic Programming optimization algorithm used the net total stress and pore-water pressure distributions to determine the location and shape of the critical slip surface and the corresponding factor of safety.

4.1 Problem Geometry, Initial, and Boundary Conditions

Figure 4 presents the geometry, boundary conditions, and initial conditions of the embankment studied. The embankment has a side slope at 1.5H:1.0V and a height of 10 m. The initial water table is horizontal and at 8 meters of depth. A hydrostatic initial pore-water distribution is based on an assumed water table. The

boundary conditions used in the solution of Eq. 6 are presented on Fig. 4. The pore-water pressure at the embankment surface is given a value of 0 kPa, reflecting a condition where the amount of rainfall is greater or equal to the amount of water infiltrating. This rather simple atmospheric boundary condition is adequate for the analysis at hand. However, more elaborate boundary conditions can be used in situations where the ratio between the amount of rainfall and the amount of water infiltrating are changing with time. Figure 4 show that a 'no flow' boundary condition was applied on the subsurface mesh boundary. This boundary condition corresponds to a situation where the area subjected to the atmospheric boundary condition is significantly larger than the problem area and the gradients exist the subsurface mesh boundary are small.

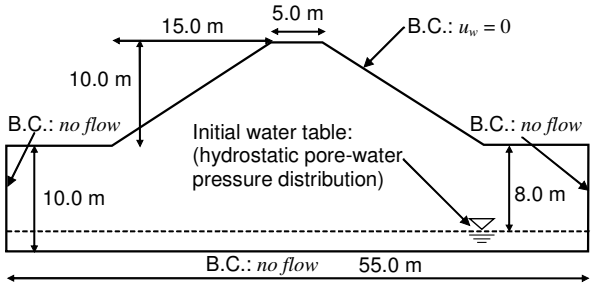

Figure 4. Problem geometry, boundary conditions, and initial values.

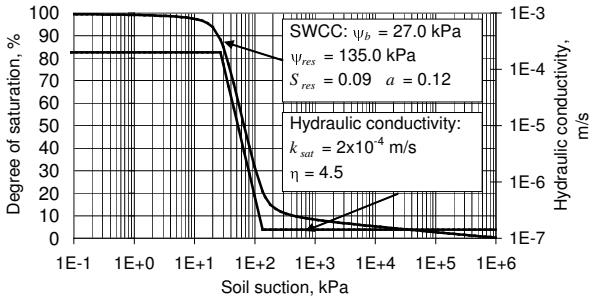

Figure 5. Soil-water characteristic curve and hydraulic conductivity functions for a lacustrine silt.

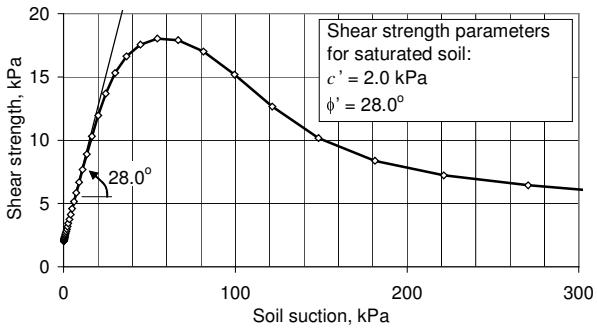

Figure 6. Shear strength for a lacustrine silt.

The boundary conditions used in the solution of Eqs. 7 and 8 are similar to the boundary conditions presented on Fig. 1. No vertical displacement restriction was applied at the sides of the finite element mesh, in order to perform a 'switch on gravity' stress analysis. The unit weight used in the stress analysis was calculated based on the degree of saturation and the void ratio and using G_s = 2.65.

4.2 Soil Properties

The properties utilised in the analyses are assumed values for a lacustrine silt. Figure 5 presents the soil-water characteristic curve (SWCC) and the hydraulic conductivity function. The unimodal SWCC presented on Fig 5. is defined by four soil parameters; namely, the air-entry value, ψ_b, the residual suction, ψ_{res}, the residual degree of saturation, S_{res}, and a parameter defining the sharpness of the transition at the bending points, '*a*' (Gitirana Jr. & Fredlund 2003). A void ratio of 0.67 was assumed. The hydraulic conductivity function was determined based on the SWCC, using the Brooks and Corey (1965) mechanistic model. A saturated hydraulic conductivity of 2x10^{-4} m/s was used.

The shear strength parameters utilised throughout the analyses are: ϕ' = 28° and c' = 2 kPa. The change in shear strength for different soil suctions was predicted using the soil-water characteristic curve and the saturated shear strength parameters, c' and ϕ'. Theoretical models supported by experimental evidence show that the slope of the plot of shear strength versus soil suction, ϕ^b, begins to deviate from the effective angle of internal friction as the soil desaturates. This reduced slope is associated with the increasingly reduction in the effective wetted area of contact past the air-entry value, as follows (Vanapalli et al. 1996):

$$\tau_f = c' + (\sigma_n - u_a)\tan\phi' + (u_a - u_w)\Theta_e \tan\phi' \quad [9]$$

where $\Theta_e = (S - S_{res})/(1 - S_{res})$. The parameters of Eq. 9 are the saturated shear strength parameters and the soil-water characteristic curve parameters presented on Fig. 5. Figure 6 presents the values of shear strength vs. soil

suction, based on Eq. 9 and used with the shear strength parameters for the lacustrine silt.

4.3 Stability Analysis Results

Figure 7 presents a typical pore-water pressure distribution after a considerable amount of infiltration has occurred. The water table has risen to the soil surface at the foot of the slope. A core of unsaturated soil is still present inside the embankment, reflecting substantial water storage capability at the center of the problem. Pore-water pressure distributions for additional time steps are not presented herein, but the evolution of the water table can be seen on Figs. 8, 9, and 10.

The search grid formed by grid cells of 1.00 m (H) by 0.25 m (V) was used in the Dynamic Programming analysis. For the search grid used, the computation time varies between 5 and 10 seconds on a Pentium IV-M running at 1.8 GHz and with 512mb of RAM. The finite element computations vary from 5 to 20 seconds, with the longer times corresponding to analysis using higher Poisson ratios. Convergence was achieved for all Dynamic Programming runs. Slip surfaces with acceptable shapes (without kinks, convex shapes, etc.) were found for all analyses. Some of the critical slip surfaces obtained deviate considerably from a circular shape, notably those presented on Fig. 8.

None of the obtained slip surfaces presented on Figs. 8, 9, and 10 are near the location where the search grid boundary crosses the face of the slope. Therefore, the chosen location where the search grid crosses the soil did not impose a restriction to the slip surface location. Special care regarding this type of restriction applied to the slip surface must be taken in problems where shallow slip surfaces are expected (i.e., problems involving cohesionless soils). Baker (1980) and the subsequent researchers have maintained the use of a search grid crossing the slope face as a requirement of the DP analytical procedure. This requirement has not interfered with the analysis here presented, even after the soil has reached saturation and with a low effective cohesion of 2 kPa.

Pham et al. (2002) found that the Poisson ratio has a significant influence on the factor of safety obtained using the DPM combined with finite element stress fields while the Young modulus has little or no influence. Therefore, the transient seepage and stability analyses were performed for three values of the Poisson ratio (μ = 0.333, 0.43, and 0.49). The Poisson ratio used in a 'switch on gravity' analysis partially controls the assumed value of K_0 ($K_0 = \mu/(1-\mu)$). The values of the Poisson ratio used herein correspond to K_0 = 0.50, 0.75, and 1.00, respectively.

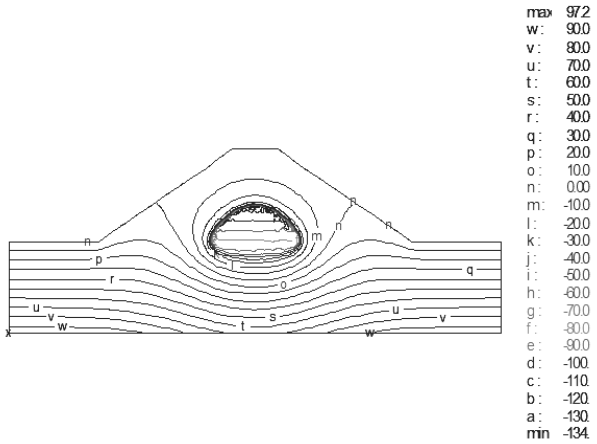

Figure 7. Typical pore-water pressure distribution after strong rainfall (t = 72 hours).

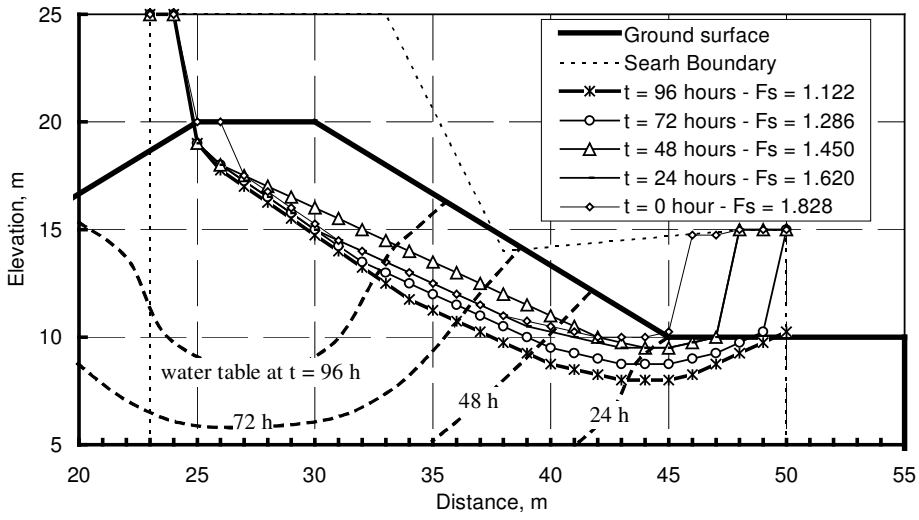

Figure 8. Slip surfaces for Poisson ratio = 0.333.

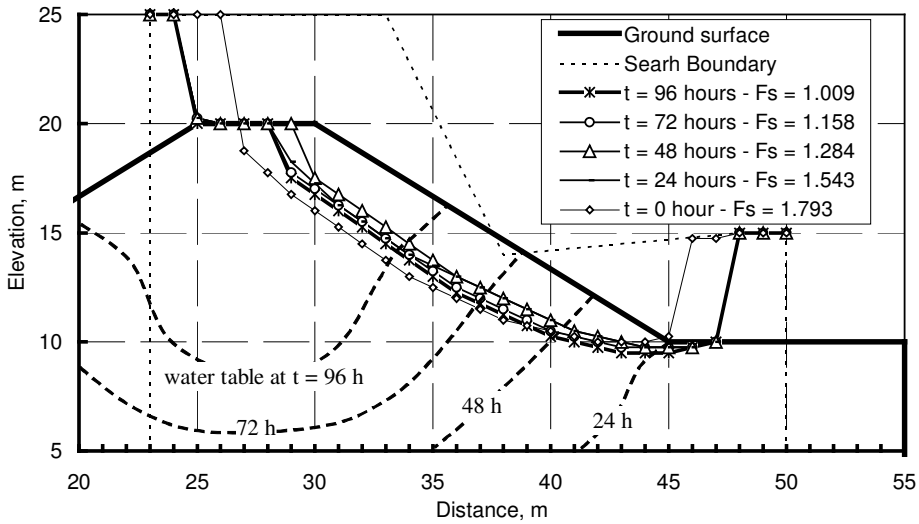

Figure 9. Slip surfaces for Poisson ratio = 0.43.

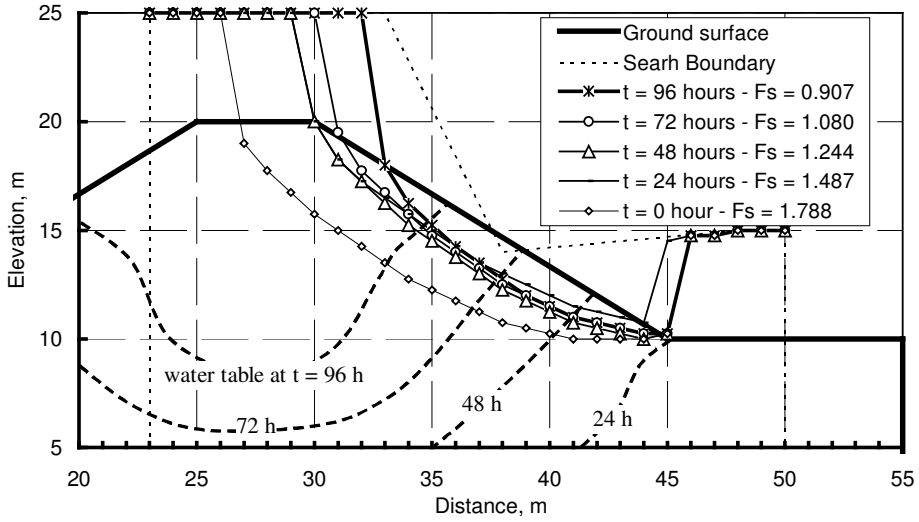

Figure 10. Slip surfaces for Poisson ratio = 0.49.

The embankment stress distribution is not entirely under K_0 conditions. Therefore, while 'more confined' regions of the embankment have σ_y/σ_x ratios higher than K_0, regions close to the slope surface have σ_x/σ_y ratios lower than K_0. The overall effect of the value of μ used is reflected by the higher σ_x/σ_y ratios (closer to 1) inside the embankment for larger μ values. The σ_x/σ_y ratios closer to 1 inside the embankment drive the slip surfaces to shallower regions, where lower σ_x/σ_y ratios are found (i.e., higher deviatoric stresses, $\sigma_y - \sigma_x$). This overall behavior can be observed by comparing Figs. 8, 9, and 10.

Figure 10 (μ = 0.49) shows that the slip surfaces become shallower as the soil saturates and the 'apparent cohesion' (i.e., effective cohesion plus shear strength due to increases in soil suction) is reduced. This behaviour is anticipated, based on conventional limit equilibrium analyses. Figure 9 show that the effect of the reduction in 'apparent cohesion' was not evident, due to the larger deviatoric stresses inside the embankment. The result shown on Fig. 9 is more pronounced for μ = 0,333. Figure 8 shows slip surfaces becoming deeper as the soil saturates, giving the opposite tendency of what is shown on Fig. 10.

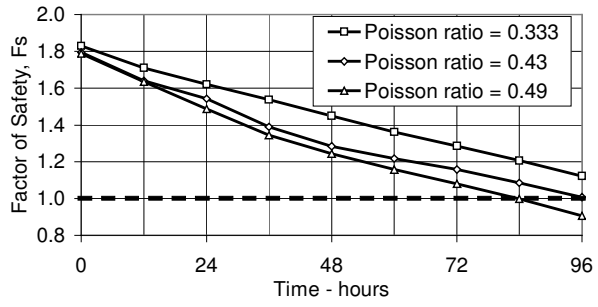

Figure 11. Factor of safety evolution with time for different Poisson ratios.

The water table rise reflecting the atmospheric boundary conditions produces a decrease in shear strength inside the embankment. The evolution of the factor of safety with time for three values of the Poisson ratio (μ = 0.333, 0.43, and 0.49) is presented on Fig 11. After 4 days the embankment reaches failure ($F_s < 1$). The use of larger Poisson ratios corresponds to lower factors of safety. As explained above, larger values of Poisson ratio produce shallower surfaces. Local factors of safety, or mobilized shear strength, can be used in the interpretation of the results. The local factors of safety near the slope face are lower, assisting in explaining the slip surface position.

5. CONCLUSIONS

The application of the *Dynamic Programming Method* to the analysis of stability of embankments subjected to transient moisture flow was presented. A hypothetical embankment comprised of lacustrine silt subjected to a continuous, heavy rainfall was analyses for a period of four days, using a dynamic Programming algorithm called SAFE-DP. The stresses and pore-water pressures were determined based on the partial differential equations governing equilibrium and moisture flow. The general purposed solver called FlexPDE (PDE Solutions Inc. 2003) was used for the finite element analyses.

The evolution of the shape and position of the slip surface and the evolution of the corresponding factors of safety is presented and analysed. The results of the analyses indicate that the DPM code is robust, fast, and stable. The stability analysis using the DPM shows that the slip surface shape is affected by the infiltration and deviates from a circular shape in some cases. Poisson ratio was found to have an important influence on the shape of critical slip surfaces and the factors of safety.

ACKNOWLEDGEMENTS

The authors would like to thank the Canadian Pacific Railway, the Natural Sciences and Engineering Research Council of Canada – NSERC, and the "Conselho Nacional de Desenvolvimento Científico e Tecnológico – CNPq, Brasil", for financial support.

REFERENCES

Baker, R. 1980. Determination of the critical slip surface in slope stability computation. International Journal for Numerical and Analytical Methods in Geomechanics, **4**: 333-359.

Bellman, R. 1957. Dynamic programming. Princeton University Press, Princeton, N.J.

Brooks, R.H. and Corey, A.T. 1964. Hydraulic properties of porous media. Colorado State University Hydrology Paper. No 3., 27 pp.

Fredlund, D.G. & Rahardjo, H. 1993. Soil Mechanics for Unsaturated Soil. John Wiley & Sons, New York, United States of America, 517 p.

Gitirana Jr, G.F.N and Fredlund, D.G. 2003. Soil-water characteristic curve equation with independent properties. *Journal of Geotechnical and Geoenvironmental Engineering, ASCE*. (submitted).

PDE Solutions Inc. 2003. FlexPDE 3.10 - Reference Manual. Antioch, CA, USA.

Pham, H.T.V. 2002. Slope stability analysis using dynamic programming combined with finite element stress analysis. M.Sc Thesis. University of Saskatchewan, Saskatoon, SK, Canada, 200 pp..

Pham, H.T.V., Fredlund, D.G., and Gitirana Jr, G.F.N. 2001. Slope stability analysis using dynamic programming combined with finite element stress analysis. *In* International Conference on Management of the Land and Water Resources – MLWR. Hanoi, Vietnan. v. 1, pp. 107-114.

Spencer, E. 1967. A method for analysis of the stability of embankments assuming parallel interslice forces. *Geotechnique*, **17**(1): 11-26.

Vanapalli, S.K., Fredlund, D.G., Pufahl, D.E. and Clifton, A.W. 1996. Model for the prediction of shear strength with respect to soil suction. Can. Geotech. J., Ottawa, **33**: 379-392.

Yamagami, T., and Ueta, Y. 1988. Search for critical slip lines in finite element stress field by dynamic programming. *In* Proceedings of the 6th International Conference on Numerical Methods in Geomechanics, Innsbruck, pp. 1347-1352.

Zou, J. Z., Williams, D. J., and Xiong, W. L. 1995. Search for critical slip surfaces based on finite element method. Canadian Geotechnical Journal, **32**: 233-246.